# Chapter 4
# Design Considerations of Small-Animal SPECT Cameras

**Steven R. Meikle, Peter L. Kench, and Jianyu Lin**

## 1 Introduction

### *1.1 Rationale for Small Animal SPECT as a Research Tool*

Single photon emission computed tomography (SPECT) is a tomographic imaging modality based on the radiotracer principle [1]. It is used to measure the 3D distribution of radiolabelled molecules in vivo using very sensitive radiation detectors and mathematical image reconstruction algorithms. Although SPECT has been used as a clinical tool for several decades, it is also well suited to imaging small animal models of human disease, such as laboratory mice and rats, for pre-clinical research. Because of the relatively long physical half-lives of single photon emitters (Table 4.1), SPECT is best suited to the study of macromolecules, such as antibodies and proteins, which have relatively slow rates of accrual at their target sites and slow plasma clearance. Additionally, proteins and antibodies are easily labelled with one of the radioisotopes of iodine ($^{125}$I, $^{123}$I or $^{131}$I), or else by attaching a chelating agent incorporating one of the other common single photon emitters with suitable imaging properties, such as $^{99m}$Tc or $^{111}$In. Conversely, the closely related radiotracer technique positron emission tomography (PET), which is discussed in the following chapter, is best suited to the study of small molecules such as synthetic drugs which have relatively fast kinetics in the body. Thus, the two techniques are highly complementary in the pre-clinical research environment.

S.R. Meikle (✉) • P.L. Kench
Faculty of Health Sciences, Brain and Mind Research Institute, University of Sydney, Sydney, NSW, Australia
e-mail: s.meikle@usyd.edu.au; peter.kench@sydney.edu.au

J. Lin
Department of Electrical and Computer Engineering, Curtin University, GPO Box U1987, Perth, WA 6845, Australia
e-mail: jianyulin@hotmail.com

H. Zaidi (ed.), *Molecular Imaging of Small Animals: Instrumentation and Applications*,
DOI 10.1007/978-1-4939-0894-3_4, 

**Table 4.1** Single photon-emitting radionuclides commonly used in small animal imaging studies and their physical characteristics

| Radionuclide | Main emission energy (keV) | Half-life |
|---|---|---|
| $^{99m}$Tc | 140 | 6.02 h |
| $^{123}$I | 159 | 13.3 h |
| $^{131}$I | 364 | 8.2 days |
| $^{125}$I | 20–35 (X-rays) | 59 days |
| $^{111}$In | 171, 245 | 2.8 days |

## *1.2 Pre-clinical Applications of SPECT*

The instruments and techniques used to acquire a small animal SPECT study are determined by the research question, the species of animal, the structure and physiology of the organ(s) of interest and the desired spatial resolution and sensitivity. The size of the smallest structure to be imaged and the activity distribution within tissue are important considerations for determining the required spatial resolution of the system [2]. Imaging of the rodent brain, myocardium, skeletal system or a tumour may have different spatial resolution and sensitivity requirements. For example, the brain is a complex structure requiring high spatial resolution and sensitivity in order to quantify radiopharmaceutical uptake in structures such as the striatum and cerebellum for studying the dopaminergic system [3, 4]. Imaging the rodent skeleton requires high spatial resolution; sensitivity is less critical, however an extended axial FOV is required to image the whole skeleton. Engrafted tumours often exhibit a heterogeneous distribution of radiopharmaceutical due to rapid tumour growth and tissue necrosis, which require high spatial resolution for accurate quantification. With appropriate collimation and detector configuration, whole body sub-millimetre spatial resolution can be achieved for rodent skeletal and tumour imaging [5].

High system sensitivity is required when investigating tracer kinetics and quantifying uptake. Many SPECT systems support dynamic acquisition for studying tracer kinetics, but reliability of kinetic parameter estimates is dependent not only on temporal resolution but also good signal to noise ratio (SNR). For cardiac and lung imaging, physiological motion may cause excessive blurring. Using a physiological trigger, such as the 'R' wave from an electrocardiograph (ECG), SPECT projections can be divided into discrete time bins that represent different parts of the physiological (e.g. cardiac) cycle. Reconstructing and sequentially displaying each frame in the cycle allows visualisation and quantification of radiopharmaceutical uptake during different phases of the periodic motion. Gated SPECT also allows quantitative analysis of myocardial contractile function and/or motion correction of the respiratory cycle.

Some applications require the capability to simultaneously image multiple radionuclides with different emission energies. For example, Zhou et al. co-injected animals with $^{111}$In-oxyquinoline labelled stem cells and $^{99m}$Tc-sestamibi, enabling simultaneous imaging of the engraftment of stem cells and perfusion defects in the infarcted rat myocardium [6]. Here, the 245 keV photons of $^{111}$In and the 140 keV

photons of $^{99m}$Tc were imaged simultaneously in separate energy windows. Such studies require good energy resolution to minimise cross-talk between radionuclide measurements.

These are just some of the very broad areas of application of small animal SPECT in preclinical research. More specific examples are given in later chapters. The key point is that the performance parameters of small animal SPECT systems are very application dependent. Therefore, the intended research applications are an important consideration in the design of small animal SPECT systems.

## 2 Design Principles

The basic unit of a SPECT system is the radiation imaging detector, also called a gamma camera. The gamma camera senses the photon emitted by a radiation source and determines the two-dimensional position of its interaction within the detector plane (in some detector designs, depth within the finite thickness of the absorber may also be encoded) and the resulting energy deposited within the detector. Thus, typically a gamma camera produces an X and Y signal representing the position coordinates of the absorbed photon and a Z signal representing its energy. The different types of radiation detector and the technologies that underpin them were described in detail in Chaps. 1 and 2. The specific choices appropriate for SPECT are discussed in Sect. 3.5 of this chapter.

In PET, the position coordinates recorded on two opposing detectors are sufficient to determine the trajectory of the annihilation photon pair. This is not the case in SPECT. The position coordinates recorded by a gamma camera tell you where the photon was absorbed but not where it came from. To determine the trajectory of the photon, another key component of the gamma camera is required—the collimator. This is a device attached to the gamma camera and constructed of material with sufficient density and thickness to absorb most of the emitted photons, allowing only a small fraction to pass through one or more open apertures and reach the detector along certain preferred trajectories. For small animal SPECT, the pinhole collimator is the most common design as it provides the best resolution-sensitivity trade-off for imaging small objects. However, there are other alternatives and there are various pinhole designs optimized for different imaging conditions. These are discussed in detail in Sec. 3.6.

Since SPECT is not affected by positron range or non-collinearity effects, it is capable of higher spatial resolution than PET, especially when pinhole collimation is employed, but at the expense of considerably lower sensitivity (approximately 1–2 orders of magnitude lower than PET). The sensitivity of SPECT can be improved by designing the collimator aperture(s) to allow more photons to pass through per unit of radioactivity, or by increasing the number of pinholes and detectors surrounding the animal. However, increased collimator sensitivity comes at the cost of poorer spatial resolution, while increasing the number of detectors increases the cost of the system. For certain types of collimation—in particular focusing

collimators, such as pinholes—sensitivity and spatial resolution can both be improved by minimizing the distance between the pinhole(s) and the subject, at the same time constraining the size of the field of view (FOV). These choices need to be carefully considered in view of the species and organs to be imaged.

Thus, the key trade-offs in SPECT system design are between sensitivity, spatial resolution and the size of the FOV, with cost being an additional, sometimes limiting, constraint. Other considerations include the requirement for quantitative measurements (e.g. absolute tracer concentrations and/or physiological parameter estimates) and the importance of accurately co-registered structural images, such as those provided by X-ray computed tomography (CT) or magnetic resonance imaging (MRI). These considerations drive choices about system configuration and integration of complementary imaging modalities. There are a number of commercial small animal SPECT systems now available, including SPECT–CT hybrid systems. Most are capable of sub-millimeter spatial resolution and have sufficient sensitivity and quantitative capability to perform studies of tracer kinetics. There remain many challenges to further improving the spatial resolution, sensitivity and functionality of preclinical SPECT systems through the development of new instrumentation, imaging techniques and data analysis algorithms. The key drivers for addressing these design challenges are discussed in the following sections.

## *2.1 Spatial Resolution Versus Sensitivity*

There is a trade-off between system spatial resolution and sensitivity which is ultimately determined by appropriate choice of detector and collimator design. The parameters of these are further constrained by several other factors such as FOV size and energy of photons. For parallel hole and pinhole collimator designs, improvements in spatial resolution are usually at the cost of sensitivity [2]. As the diameter of the collimator hole increases the number of photons that can pass through to the detector (sensitivity) also increases but the precise origin of the photon (spatial resolution) becomes more difficult to determine. Parallel collimators are sometimes useful for whole body small animal planar imaging, but the spatial resolution is limited by the intrinsic resolution of the detector, collimator design parameters and distance from the animal. Pinhole collimators are more frequently used for small animal imaging as they offer the best trade-off between spatial resolution and sensitivity for small objects [5, 7]. Magnification of the projection image due to the pinhole geometry improves the observed spatial resolution beyond the intrinsic resolution of the detector. Moving the object closer to the pinhole aperture magnifies the projection, resulting in further improvement in spatial resolution and sensitivity of the system, but at the cost of a smaller FOV as shown in Fig. 4.1. For parallel-hole collimators, the sensitivity is approximately independent of the distance between the collimator and object, as illustrated in Fig. 4.1b.

A mouse is approximately 3,000 times smaller by volume and weight than a human [8, 9]. Given that a typical clinical SPECT system has volumetric spatial

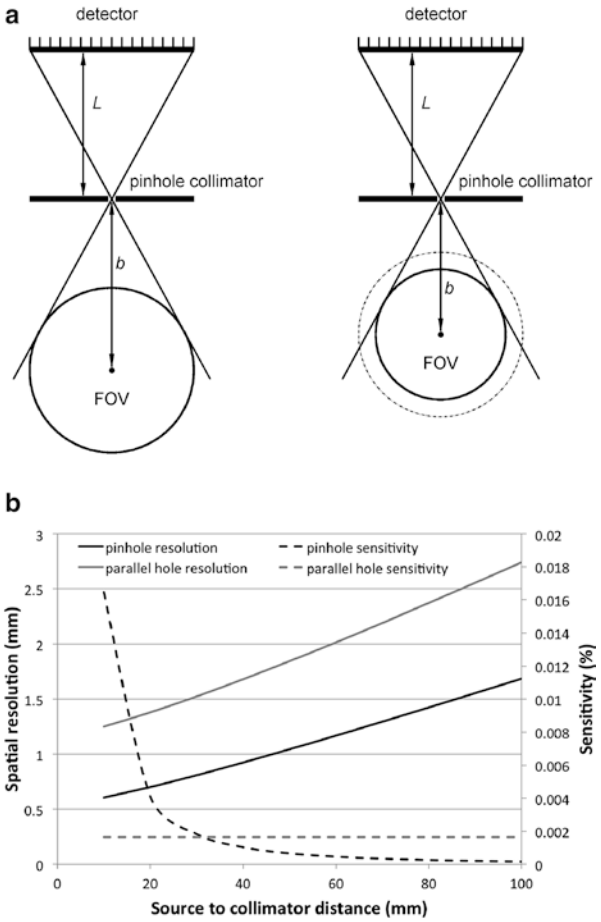


**Fig. 4.1** The effect of source to collimator distance on system spatial resolution and sensitivity for pinhole and parallel hole collimators. Intrinsic resolution of the detector is assumed to be 1 mm and the aperture diameter is 0.5 mm for the pinhole and 0.5 mm for the parallel hole collimator. Focal length of the pinhole is 80 mm while septal length and thickness of the parallel hole collimator are 25 and 0.15 mm respectively. Note that at short distances the pinhole collimator leads to both improved resolution and sensitivity compared with the parallel hole collimator, but also a reduced FOV

resolution of approximately 1 $cm^3$ at the centre of the FOV, a mouse SPECT system would require volumetric resolution of $3 \times 10^{-4}$ $cm^3$ (i.e. linear spatial resolution of 0.7 mm) in order to achieve comparable delineation of organs and structures of interest. This may seem a daunting challenge but Fig. 4.1 indicates that a target resolution of 0.7 mm can be achieved with pinhole collimation when the centre of the FOV is approximately 20 mm from the pinhole focus, a realistic distance for a mouse. The greater challenge is to acquire enough counts in each voxel to support this resolution and, thus, achieve similar signal-to-noise to a clinical SPECT study with much larger voxels.

The relatively poor sensitivity of pinhole SPECT can be offset by increasing the administered dose of radioactivity to the animal. This tends to result in higher radiation doses being administered to rodents than humans relative to their volume and mass [8]. Hence, careful consideration needs to be given to the potential impact of a high radiation dose to the animal. This is particularly true for longitudinal studies

where multiple doses of radiopharmaceutical are administered. Researchers need to be confident that SPECT measurements as a function of time are a result of disease progression or intervention and not radiation induced changes. Funk, Sun and Hasegawa estimated the whole body radiation dose for radionuclides commonly used in small animal SPECT and PET imaging [10]. The radiation dose for a mouse is generally greater than that for a rat by a factor of 10 for the same administered activity, due to its smaller body mass. They found that the whole body radiation dose in mice varied between 6 cGy and nearly 1 Gy which is only an order of magnitude less than the lethal dose (LD50/30 approx. 7 Gy) for a mouse. Thus, it is recommended to limit the radiation dose to 10 cGy or less for mice involved in longitudinal studies. The need for high spatial resolution and low radiation dose is driving the development of small animal SPECT systems with higher sensitivity.

## *2.2 The Need for Quantification*

The observed distribution of radiopharmaceutical within a small animal is usually a qualitative or semi-quantitative measure. The uptake within organs and various tissues can be visually compared to uptake in surrounding structures. The ability to provide an absolute measure of tracer concentration in tissue, and/or quantify physiological kinetic parameters, may enhance understanding of the in vivo behaviour of the radiopharmaceutical and the pathophysiology of disease. The impact of an intervention may also be better understood with quantitative measurements of tracer distribution as a function of time within the same animal. When quantification is performed the tracer distribution is expressed as absolute radioactivity or percentage of injected dose per unit tissue volume. Tracer kinetics can be observed by acquiring a dynamic sequence of tomographic data over an extended time, typically up to 90 min following administration. PET is considered ideal for such studies because of its high sensitivity and temporal resolution. Recent advances in small animal SPECT have seen greatly improved sensitivity and full ring systems making tracer kinetic studies now possible [5, 11].

The small size of a rodent makes the bias caused by photon attenuation much less than that which occurs in larger animals and humans. However, for accurate quantification, this error needs to be considered and corrected for. One approach is to assume a constant linear attenuation coefficient for the whole animal (i.e. uniform tissue density) and correct for attenuation based on the distance travelled by the gamma ray within the animal. This approach works well for soft tissue within the abdomen but problems arise when quantifying myocardial tissue uptake due to the different densities of myocardial and surrounding lung tissue. A more accurate approach is to create an attenuation map from a CT volume and correct for SPECT attenuation errors during reconstruction. The CT derived attenuation data need to be calibrated for the difference in photon energy between the X-ray source and SPECT radioisotope. The accuracy of this technique has been demonstrated in several studies (e.g. [12]).

Li et al. [13] demonstrated the feasibility of using highly magnified pinhole SPECT for quantification by accurately (<7% bias) determining the activity of point sources in air and water. The method used a filtered backprojection reconstruction algorithm that considered the impact of attenuation, scatter, pinhole geometric response and system misalignment. Acton et al. [3] quantified dopamine transporters in the mouse brain using $^{99m}$Tc TRODAT-1 and a triple detector clinical system fitted with custom made single pinhole collimators. The investigators used a simplified reference tissue model to quantify kinetic parameters [14], which had been previously validated in primates, thus avoiding the need for arterial blood sampling, which is difficult to perform in mice.

High spatial resolution is important when quantifying tissue uptake of radiopharmaceutical as borders can be clearly defined and the impact of the partial volume (PV) effect is reduced. When an imaging system has low spatial resolution, events from an adjacent projection pixel or reconstructed voxel spill in or out of the area of interest. This problem causes a loss of accuracy within the area of interest known as the PV effect. In the study by Acton et al. [3] the pinhole SPECT spatial resolution was 0.83 mm at 30 mm radius of rotation, which is better than can be achieved with current small animal PET systems. The in vivo SPECT tissue uptake measurements correlated strongly with ex vivo tissue counting, validating the quantification method used. The test–retest value was a low 2.6 %, indicating that this method is a useful technique for longitudinal studies. Future improvements in the sensitivity of small animal SPECT systems will allow shorter time frames between acquisitions and include anatomical localisation for correctly identifying tissue boundaries.

In summary, quantitative errors can be corrected in small animal imaging but their magnitude is influenced by the spatial and energy resolution of the SPECT system, the choice of radionuclide and the geometry of the radiopharmaceutical distribution within the animal.

## *2.3 The Need for Anatomical Localisation*

It is desirable to localise foci of increased or decreased radiopharmaceutical uptake in relation to surrounding anatomical structures to ensure correct interpretation of the image. It is often the case that radiopharmaceuticals with high specificity for their target site also exhibit less non-specific uptake in surrounding organs and tissues. Paradoxically, radiopharmaceuticals with a lot of non-specific uptake in surrounding tissues provide information that helps to localize uptake in the target tissues.

Methods of identifying the localisation of a radiopharmaceutical include using external markers or the administration of a second radiopharmaceutical with different pattern of uptake. Placing an external radionuclide marker on the animal in a known location provides a reference point for identifying radiopharmaceutical uptake. External markers can be difficult to secure to the animal's fur or skin but are an easy method for providing a gross estimate of radiopharmaceutical location.

Administering a different radiopharmaceutical that localises within or adjacent to the organ of interest can provide a more accurate method of localisation. If radionuclides with the same or similar photon energies are used, the study of primary importance to the research question should be performed prior to administration of the radiopharmaceutical for anatomical localisation. If the radiopharmaceuticals have quite different photon energies then simultaneous dual isotope imaging can be performed [6]. It is desirable for the radiopharmaceutical of interest to have the higher photon energy to minimise Compton or 'down' scatter into the lower energy window, which would otherwise reduce the quality of the SPECT study.

It is becoming increasingly important in research applications to accurately localise radiopharmaceutical biodistribution relative to known anatomical structures, particularly for new targeted radiopharmaceuticals with low non-specific binding. X-ray CT and MRI can provide detailed anatomical information which is highly complementary to the SPECT study. Thus, it is common in commercial systems for SPECT to be one component of a dual- or even tri-modality imaging system. There are several possible combinations and approaches to multi-modality imaging which are discussed in later chapters, including SPECT/CT (Chap. 12) and SPECT/MRI (Chap. 14). The detector developments that give rise to these possibilities are discussed in Chaps. 2 and 3.

## 3 System Design

### *3.1 Angular Sampling*

To perform SPECT, multiple projections must be acquired from a large number of uniformly spaced angles around the subject. Certain conditions for the acquisition geometry must be met for the projection data to be successfully reconstructed into a volume representing the distribution of radiopharmaceutical. Orlov and Tuy described the geometrical requirements for parallel hole and pinhole tomography respectively [15, 16]. For a successful SPECT reconstruction, the volume of interest must be fully sampled in each of the projections, i.e. the volume must not be truncated, otherwise reconstruction artefacts may result. Additionally, Tuy's condition states that for pinhole SPECT (or any other cone beam geometry), the pinhole focus must trace out an arc of a great circle as the detector rotates around the subject in order to obtain an accurate reconstruction [15]. In the case of single pinhole SPECT, this condition is only satisfied for the central slice through the subject that is coplanar with the pinhole aperture. Multiple pinhole collimation can be used to overcome this limitation, as discussed below.

A key consideration is the number of projection angles around the object, referred to as angular sampling, which may affect the quality of the reconstructed SPECT volume. For SPECT systems there is a trade-off between the number of projection angles and the acquisition time for each projection. If the time for each projection is

too short the data will contain increased noise relative to signal, resulting in poor reconstruction results. The kinetics of the radiopharmaceutical, injected activity, system sensitivity and duration of anaesthesia all limit the total SPECT acquisition time and, hence, limit the acquisition time per projection and/or number of projections.

Sufficient angular sampling for SPECT can be achieved by rotating the detector around a stationary animal [17], rotating the animal in front of a stationary detector [18] or completely surrounding the animal with stationary detectors [5, 19]. From Shannon's sampling theorem [20], it is necessary to sample at least twice the achievable spatial resolution to ensure resolution is not degraded. The optimal number of projections to faithfully reconstruct the object and prevent angular under sampling for the available spatial resolution is therefore given by:

$$N = \pi D \Big/ \left( \frac{\delta x}{2} \right) \tag{4.1}$$

where $D$ is the diameter of the FOV (or object of interest centred on the AOR) and $\delta x$ is the system spatial resolution [21, 22].

To increase the FOV the animal can be translated in the axial and/or transaxial directions through the focal area of the detector(s) during SPECT acquisition. Since the locations of the detector and animal are known for each projection the lines of response can be determined allowing the extended FOV to be reconstructed into a larger volume.

## *3.2 Retrofitted Clinical SPECT Systems*

The initial feasibility studies of small animal pinhole SPECT imaging were performed using human SPECT systems [23]. Clinical SPECT systems usually have one or more rectangular or round monolithic inorganic scintillation crystals, each 300–500 mm wide, coupled to an array of single anode photomultiplier tubes (PMT). When a gamma ray interacts with the scintillation crystal some or all of the energy is transferred into visible light. The number of light photons is proportional to the energy deposited in the scintillation crystal. The location and energy of a scintillation within the crystal is determined by analyzing the relative intensity of signals produced in the PMTs directly beneath and surrounding the event, a method known as 'Anger Logic' [24].

Early small animal SPECT imaging studies used existing clinical SPECT systems retrofitted with specially designed pinhole collimators to obtain high spatial resolution and sensitivity for small animal imaging [25]. To overcome the low intrinsic spatial resolution of a clinical pinhole SPECT system, a large magnification factor must be used. The use of a clinical SPECT system fitted with a small aperture pinhole collimator provides a cost effective method of small animal SPECT imaging, as the cost of new equipment and ongoing maintenance are avoided. The large surface of the detector allows for highly magnified projections, and placing the

animal close to the pinhole produces reasonable sensitivity. Unfortunately, there is some loss of spatial resolution near the edge of the detector due to parallax error caused by the oblique incidence angle of the photon and the finite thickness of the crystal. Because clinical SPECT systems are optimised for photon energies of 140–300 keV they are not well suited to small animal studies using low photon energy radionuclides such as $^{125}$I (20–35 keV) which produce low light output within the crystal. When a SPECT system is used for human and small animal imaging, careful consideration needs to be given to scheduling of studies and regulatory requirements for shared human and animal imaging equipment. The size and cost of a clinical SPECT system make it less than ideal for a dedicated small animal imaging facility [26].

### *3.3 Systems Based on Compact High Resolution Detectors*

The need for dedicated small animal SPECT and breast imaging systems resulted in the development of radiation detectors with higher intrinsic spatial resolution [27, 28]. This was achieved by developing new approaches in PMT and inorganic scintillation crystal designs. The array of single anode PMTs used in a clinical SPECT system was replaced by one or more position sensitive PMTs (PS-PMT) which are capable of very high intrinsic spatial resolution. These devices, which are discussed in detail in Chap. 3, have multiple anodes whose outputs are used to calculate an X and Y position signal for each detected scintillation event. The sum of the signals from all anodes is proportional to the number of light photons detected in the photocathode, hence the energy of the gamma ray absorbed in the crystal. A limitation of PS-PMTs is their relatively poor uniformity and linearity of response, particularly near the edge. However, their spatial response is very stable over time. A linearity correction or event position lookup map is created to ensure that all events are mapped to the correct position.

To further improve spatial resolution the scintillation crystal can be made thinner. With decreasing crystal thickness, the light from a scintillation event is better localised, but at the cost of reduced detection efficiency. There is also an improvement in energy resolution and a decrease in the non-linear edge effects when the diameter/thickness ratio of an inorganic scintillation crystal disc is increased. Wirrwar et al. [29] recommend scintillation crystal diameter/thickness ratios to be greater than 30 for new detector designs.

A pixelated crystal array comprising small (typically 1–2 mm wide) tightly packed crystals is an alternative approach to achieving high intrinsic spatial resolution. The crystal needles in a pixelated array are separated by a reflective material such as Teflon to prevent scintillation light from escaping to adjacent crystals and to reflect light photons from within the crystal towards the photocathode of the PMT. As the width of the crystal needle decreases the amount of packing material becomes a larger percentage of the total detector area, resulting in loss of detection efficiency. The distance between the centres of adjacent crystals (crystal pitch) includes the

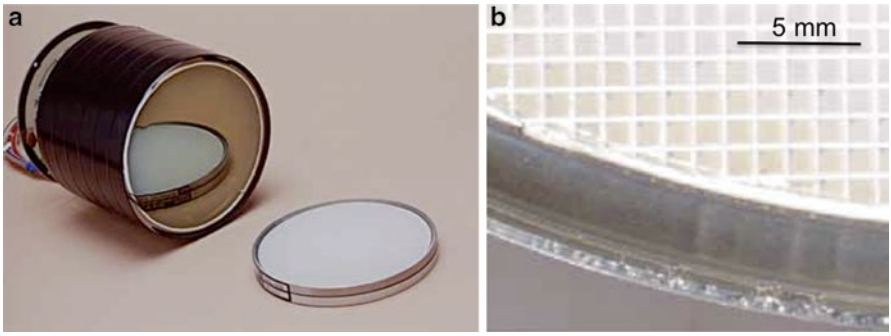


**Fig. 4.2** (**a**) Hamamatsu R3292-02 PS-PMT and pixelated NaI(Tl) crystal array. (**b**) A zoomed section of the crystal array showing individual elements and reflective packing. The array comprises 1 mm crystals on a 1.25 mm pitch

crystal width and packing material. The intrinsic spatial resolution of the detector is approximately the same as the crystal pitch, provided it is coupled to a high resolution detector such as a PS-PMT (Fig. 4.2). Since the individual crystal needles of a multiple crystal array are precisely positioned, a map of all crystal locations can be used to correct for the non-linear response of the PS-PMT. Scintillation events are assigned to the location of individual crystals based on the measured map of crystal locations derived from a high count flood acquisition. It is desirable to make the crystal pitch small (e.g. 1 mm or less) for high resolution but the needles must be sufficiently thick to absorb most photons for good detection efficiency. However, as the crystal needle length-to-width ratio increases light output decreases due to internal reflections resulting in a loss of energy resolution [26, 29, 30].

## *3.4 Rotating Versus Stationary SPECT Systems*

A variety of SPECT system designs are used to acquire sufficient angular samples of the animal for tomography. These include rotating or translating animals in front of a stationary collimator and detector, rotating collimators with stationary detector(s) and animal, rotating detectors and collimators with a stationary animal, and completely stationary systems (Fig. 4.3). Each design has specific advantages and disadvantages that need to be considered.

The simplest small animal SPECT system involves the vertical or horizontal rotation of the anaesthetised animal in front of a stationary detector [31]. The design should allow the AOR to be centred over the pinhole. The animal gantry needs to be rotated through at least 180° using incremental steps. Vertical rotation is preferred over horizontal rotation to reduce the chance of organ movement during the scan, although horizontal rotation systems have also been developed that address the organ motion issue [18]. Vertical positioning should be done for short periods of

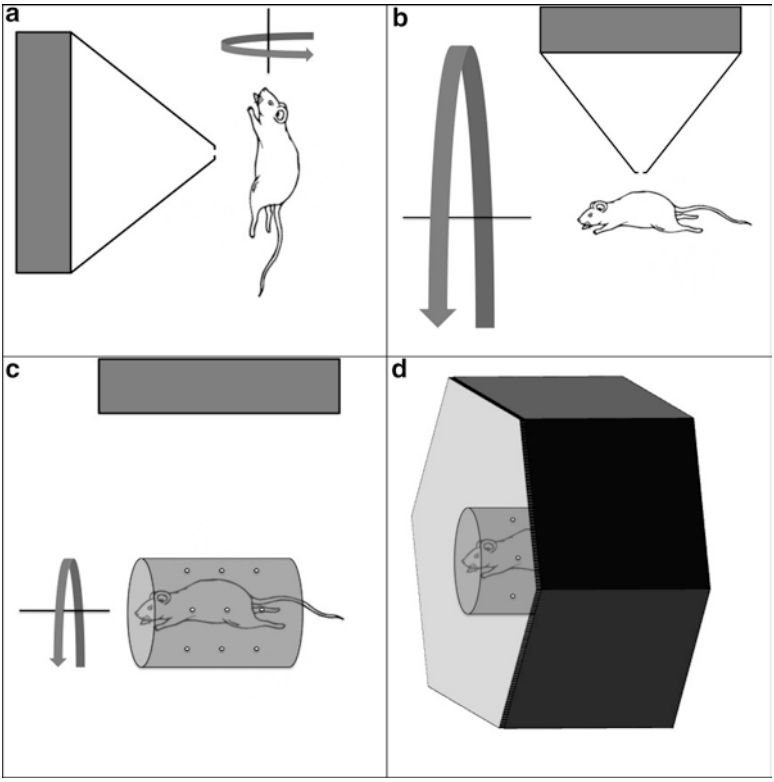


**Fig. 4.3** The common SPECT system designs are illustrated. These include systems where (**a**) the mouse rotates in front of a stationary detector and collimator, (**b**) the detector and collimator rotate around a stationary animal, (**c**) the collimator and the animal rotates in front of a stationary detector and (**d**) the system and animal are stationary

time only, as it is not well suited to the rodent's physiology and has been related to an increased incidence of mortality [32]. The advantage of rotating the animal instead of the SPECT detector is that the weight of the animal is considerably less than that of the detector and the gantry is simpler and cheaper to design. The weight of a detector with collimation and shielding may introduce mechanical misalignments resulting in reconstruction artefacts when the detector is rotated around the animal [18]. The drawbacks of rotating the animal are difficulties with accommodating apparatus for gas anaesthesia and physiological monitoring and positioning may be difficult to reproduce for longitudinal studies.

Most clinical and small animal SPECT systems have the detector and collimator mounted on a gantry that rotates 360° around the subject in precise incremental steps or continuous motion. The gantry allows the detector and collimator to move in and out perpendicular to the AOR, to adjust the radius of rotation and hence the projection magnification when pinhole collimation is used. Magnification may also be altered by changing the distance between the pinhole collimator aperture and the

detector surface [33]. The gantry must be sturdy enough to rotate the detectors without varying the radius of rotation or causing the detectors to sag. The detector must be precisely positioned to ensure that its surface is parallel and centred over the AOR. The incremental angular rotation and translation of the detector must also be precise and reproducible over extended periods of time. These engineering requirements add to the cost of designing, building and maintaining a small animal SPECT based on rotating detectors.

To improve the sensitivity and reduce the imaging times of a small animal imaging system additional detectors may be added. Multiple detector SPECT systems using two, three or four rotating detectors have been developed [3, 33–37]. Multiple detector systems reduce the need for a system to acquire projection data over a full 180° or 360°. The uniformity and sensitivity must be similar for each detector to ensure that reconstruction artefacts are not introduced. Each additional detector adds weight to the gantry and cost to the system, although multiple equally placed detectors may help to balance the gantry as it rotates.

The FOV is often limited for small animal pinhole SPECT systems that use high magnification or small compact detectors. Some imaging protocols require a greater FOV to image a larger organ such as the rat skeleton. The FOV can be enlarged by increasing the radius of rotation but this also reduces the spatial resolution and sensitivity of pinhole systems. Another approach is to move the animal stepwise through the FOV during the SPECT acquisition allowing a degree of projection overlap. The acquired data can be reconstructed separately and the volumes stitched together or the entire dataset can be reconstructed as one extended volume (Fig. 4.4) [5]. In the case of a rotating SPECT system, translating the animal in the axial direction while acquiring projection data results in the detectors travelling in a helical path around the AOR. Stepwise or helical acquisition not only increases the FOV but also reduces the incomplete sampling artefact in the axial direction sometimes observed in highly magnified circular SPECT orbits. Increasing the number of detectors for helical SPECT acquisitions also increases the likelihood of an object being sampled close to a pinhole aperture. Thus, the use of multiple detectors and a helical SPECT orbit can produce a more uniform reconstruction volume, better sensitivity and improved resolution.

Several systems have been developed with stationary detectors that surround the animal and multiple stationary or rotating pinholes. Surrounding the animal with detectors and pinholes improves system sensitivity, and rotating the collimator instead of the detector reduces gantry construction costs and avoids mechanical misalignments due to gantry rotation. For example, Goertzen et al. modified a human brain scanner, the Ceraspect, with a rotating multiple pinhole tungsten collimator insert [19]. The Ceraspect has a ring of stationary NaI(Tl) inorganic scintillation crystals coupled to PMTs. The rotating tungsten pinhole collimator has $8 \times 1$ mm$^2$ aperture pinholes evenly spaced with non-overlapping projections, and requires only a 45° rotation which can be completed in 1.25 s. The reconstructed spatial resolution measures 1.7 mm FWHM with a sensitivity of 373 counts s$^{-1}$ MBq$^{-1}$ (or 0.00037 %) with a transaxial FOV suitable for mouse imaging.

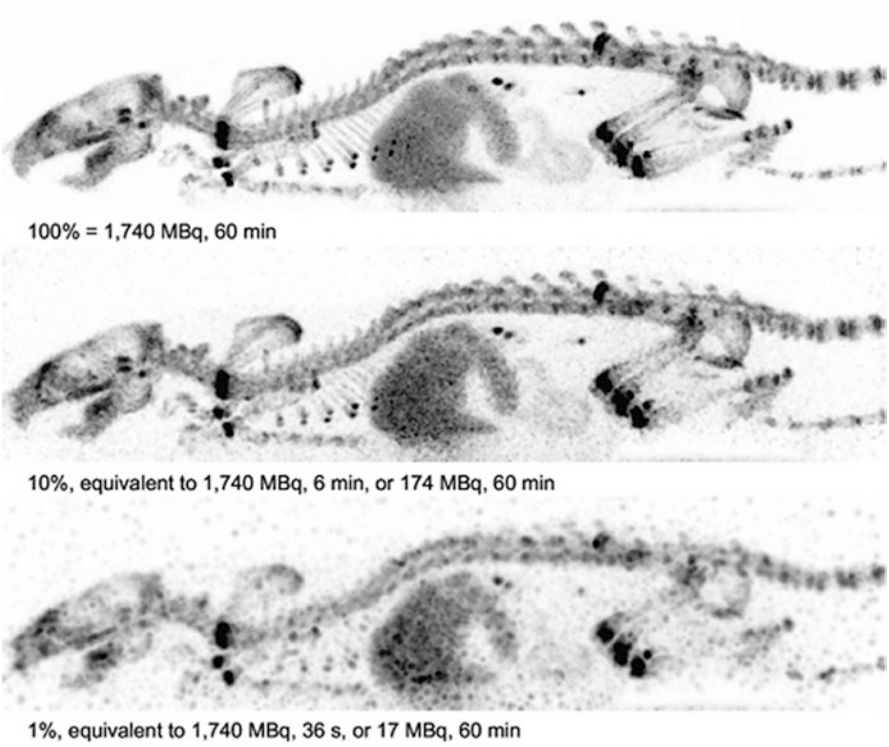


**Fig. 4.4** Whole body $^{99m}$Tc-HDP bone SPECT study of a rat. Images were reconstructed using 100 % (*top*), 10 % (*middle*) and 1% (*bottom*) of available counts from list-mode data (reproduced from [5] with permission of the Society of Nuclear Medicine)

Furenlid et al. [38] developed a stationary small animal SPECT system (FastSPECT II) based on 16 fixed individual pinhole collimators and detectors capable of imaging a mouse with photon collection efficiency of 0.04 %. Beekman et al. [11] described a small animal SPECT system (U-SPECT I) based on three stationary clinical detectors and a cylinder with five rows of 15 gold pinholes focused towards the centre of the cylinder. Projection overlap was avoided by placing additional shielding between the pinhole and the detector. Peak sensitivity is as high as 0.22 % using 0.6 mm aperture pinholes for a mouse sized collimator, making dynamic SPECT feasible. The detectors have intrinsic spatial resolution of 3.2 mm FWHM but the reconstructed spatial resolution is sub-millimetre. Since the pinholes are focused, the FOV for a single bed position is limited to 10.5 mm diameter (transaxial) and 5 mm axial [5]. Imaging larger organs or a whole body requires imaging at multiple bed positions. van der Have et al. [5] reported the sensitivity and spatial resolution of the U-SPECT II, a commercial stationary small animal SPECT system. Sensitivity was measured to be 1,500 and 525 counts $s^{-1}$ $MBq^{-1}$ for the 0.6 and 0.35 mm aperture collimators respectively. Whole body imaging is achieved by moving the animal through the focal spot of the multiple pinhole collimator using a

computer controlled system that can translate the bed in three directions. An important advantage of stationary SPECT systems is that all the required projections are acquired simultaneously, eliminating reconstruction errors due to redistribution of the radiopharmaceutical [38]. SPECT systems without moving detectors or collimators also have more stable geometric calibration and are less susceptible to mechanical misalignments.

## *3.5 Detector Choice*

The ideal detector would have 100 % likelihood of absorbing the full energy of an incident gamma ray within a small volume via a single photoelectric interaction and it would release a large number of light photons at a wavelength that matches the peak sensitivity of the photodetector.

Scintillation detectors are constructed of an inorganic crystal coupled to one or more photodetectors via a light guide. The most common inorganic scintillation crystals are sodium iodide doped with thallium [NaI(Tl)] and caesium iodide doped with thallium [CsI(Tl)] or sodium [CsI(Na)]. The thallium and sodium impurity atoms create an 'activity centre' within the crystal matrix which allows scintillation to occur at room temperature. Important properties of scintillation crystals include density, light decay time, light yield and wave length, refractive index and environmental stability. These properties are discussed in detail in Chap. 1, including the scintillation properties of the common SPECT scintillators NaI(Tl), CsI(Tl) and CsI(Na).

NaI(Tl) is a good scintillator for SPECT due to its stopping power for 140 keV gamma rays, high light output and the close match between its 410 nm emission wavelength and the peak efficiency of bialkali PMTs. CsI(Tl) has greater density and light output but slower decay time than NaI(Tl). They have a similar refractive index but CsI(Tl) is only slightly hygroscopic, making it less likely to deteriorate over time. CsI(Na) exhibits the best characteristics of NaI(Tl) and CsI(Tl) but has a longer decay time, which may be a problem for high count rate applications. Inorganic scintillators must be coupled to a photodetector, usually via a light guide matched to the refractive index of the crystal that converts light photons into an electrical signal. The most common photodetectors are PMTs (and PS-PMTs), silicon photodiodes and charge coupled devices (CCDs). PMTs have reasonable quantum efficiency (15–40 %) for converting light photons into photoelectrons, which is required for good spatial and energy resolution. Photodiodes are efficient at converting light into electrical current but produce very weak noisy signals, especially when the detectors are larger than a few mm. Geiger-mode APDs show significant promise as alternatives to PS-PMTs as they have similar gain to PMTs ($10^5$–$10^7$), fast timing properties and are MRI-compatible. Improvements in performance of CCDs make these devices viable alternatives to PMTs. Modern CCDs do not suffer from dark current when modestly cooled, and achieve quantum efficiencies as high as 90 %. Some CCDs are suitable for both optical (bioluminescence and/or fluorescence) and SPECT imaging with suitable modifications [26].

Recent developments in semiconductor radiation imaging detectors make them a viable choice for small animal SPECT in place of inorganic scintillators coupled to photodetectors. Semiconductor detectors are solid state ionisation chambers that produce one ionisation event per 3–5 keV of photon energy absorbed. Materials commonly used as semiconductors for radiation detection are silicon (Si), germanium (Ge) and, more recently, cadmium telluride (CdTe) or cadmium zinc telluride (CZT). Silicon and germanium semiconductors have similar densities (2.33 and 5.32 g $cm^{-3}$ respectively) to inorganic crystals, hence similar probability of a gamma ray interaction. However, they are not suitable for imaging due to the high thermal noise generated when operated at room temperature, making ionizing events difficult to distinguish from the background noise.

CZT, on the other hand, is a high density semiconductor material (6.06 g $cm^{-3}$) with good performance at room temperature. The probability of interaction for a 140 keV gamma ray is 83 % for 5.0 mm of CZT and energy resolution is approximately 6–7 % for a typical array element, which is better than the energy resolution of similar sized scintillation array detectors [39, 40]. CZT detectors have the added advantage of being insensitive to magnetic field strengths of up to 7 T, making them a suitable choice for hybrid SPECT/MRI systems.

## *3.6 Collimation*

The purpose of collimation is to restrict gamma rays impinging on the detector to those travelling in certain preferred and, therefore, known directions. Collimators are constructed from gamma ray absorbing material which has a high atomic number and electron density, such as lead, tungsten, gold and depleted uranium. There are a wide variety of collimator designs which provide different trade-offs between spatial resolution and detection efficiency. They can be broadly categorized as multi-channel, pinhole and slit–slat collimators.

### 3.6.1 Multi-Channel Collimation

Multi-channel collimators are constructed from a series of adjacent channels or tubes within gamma ray absorbing material that covers the entire surface of the detector. The channels may be circular, square or hexagonal. They may be drilled, die-cast or constructed from foil. Lead alloy is most commonly used for collimator construction due to its high gamma ray absorption properties, machinability and cost effectiveness. Factors that affect the spatial resolution and geometric efficiency (sensitivity) of a multi-channel collimator include the septal (wall) thickness, hole width and height of the channel. The septal wall needs to be sufficiently thick to prevent gamma rays from passing through the channel wall and interacting with the detector material. However, increased septal thickness decreases geometric

efficiency and spatial resolution. Decreasing the channel width and increasing its length increases spatial resolution but at the cost of geometric efficiency, so the choice of collimator parameters is a trade-off between spatial resolution and efficiency.

The multi-channel parallel hole collimator is designed with all the channels parallel to each other and perpendicular to the detector surface. This configuration allows only gamma rays travelling perpendicular to the detector surface and parallel to the channels to be detected. When the distance between the source of radiation and collimator is increased there is a loss of spatial resolution but the geometric efficiency of the collimator remains constant. Resolution decreases because gamma rays travelling at a larger acceptance angle from the source can now pass through more channels, resulting in a loss of detail about the photon's origin. Geometric efficiency remains stable within a range of distances because photon intensity is inversely related to distance from the source but this is offset by the increasing number of channels "seen" by the source as distance increases. The channels can be arranged so that they are all not aligned in the same direction and the channel width can vary along its length. Collimators that magnify the projection of radionuclide distribution onto the detector surface are referred to as converging or fan-beam and those that minify the projection are diverging.

The application of multi-channel collimators to small animal imaging has been limited due to their inferior spatial resolution and geometric efficiency compared with pinhole collimation for small sources. The parallel-hole collimator cannot achieve spatial resolution greater than the intrinsic spatial resolution of the detector, in fact normally it is substantially worse. The magnification of the converging collimator could increase the detector's spatial resolution, but other types of magnifying small animal collimators achieve higher geometric efficiency for objects less than 30 mm in size [41]. The multi-channel parallel collimator is, however, suitable for whole body rodent imaging using compact high resolution detectors as it does not require the animal to be translated through the FOV.

### 3.6.2 Pinhole Collimation

The main factors that influence spatial resolution and sensitivity in pinhole SPECT are magnification, aperture diameter, the distances between the source and pinhole and pinhole to detector, and the number of pinholes. Other influencing factors include the acceptance angle, the shape of the pinhole edge profile and collimator material. The ability of the pinhole collimator to magnify the projection view of the object compensates for the limited intrinsic resolution of the detector. Magnification occurs when the distance $b$ from the pinhole centre to the AOR is smaller than the distance from the pinhole centre to the detector, i.e. the focal distance $L$ (Fig. 4.1). The magnification factor is given by

$$M = \frac{L}{b} \tag{4.2}$$


**Fig. 4.5** Cross sections of pinhole collimators with (**a**) knife and (**b**) keel edges

Moving the animal closer to the pinhole has the added advantage of improving system sensitivity but this also decreases the FOV.

The contribution of the pinhole collimator to spatial resolution $R_{coll}$ and efficiency $g$ of the imaging system are proportional to the pinhole aperture diameter $d$. When calculating the $R_{coll}$ and $g$ for a pinhole collimator it is necessary to take into account the penetration of gamma rays through the knife edge of the pinhole (Fig. 4.5a) by using the effective pinhole aperture diameter $d_{eff}$ instead of $d$:

$$d_{eff} = \sqrt{d\left[d + 2\mu^{-1}\tan\left(\alpha/2\right)\right]} \tag{4.3}$$

$$R_{coll} \approx d_{eff}\left(1 + \frac{1}{M}\right) \tag{4.4}$$

$$g \approx d_{eff}\frac{\cos^3\theta}{16b^2} \tag{4.5}$$

where $\alpha$ is the acceptance angle of the pinhole opening, $\mu$ is the linear attenuation coefficient of the pinhole material for the energy of the gamma ray being imaged and $\theta$ is the angle the photon trajectory subtends with the pinhole axis, i.e. the angle of incidence.

Materials proposed for pinhole collimation include tungsten, lead, gold, platinum and depleted uranium. Lead has less attenuation than tungsten, and gold and platinum are expensive compared to tungsten alloy. The cost of gold and platinum pinholes can be reduced by creating small pinhole inserts within a tungsten plate [11, 42]. Pure tungsten has an atomic number of 74 and density of 19.3 g cm$^{-3}$ but is a difficult material to machine. However, tungsten alloys containing small amounts of Fe, Ni and Cu have favourable machining properties for collimator manufacture with a density of 18.5 g cm$^{-3}$ and a linear attenuation coefficient of 34.48 cm$^{-1}$ for 140 keV gamma rays [43]. The tenth value thickness (ln10/μ) for tungsten alloy with a 140 keV photon is 0.67 mm.

Keel-edge pinholes are recommended for medium energy (approx. 200–380 keV) photons and high resolution imaging, as the extra thickness of the edge reduces penetration [44]. They are constructed with a small channel instead of a knife edge (Fig. 4.5). With a keel-edge, sensitivity decreases as the angle between the source and the central axis of the collimator increases due to narrowing of the apparent

aperture. The geometric response of a keel-edge pinhole collimators is, therefore, different from that of a knife-edge pinhole which should be considered when reconstructing projections from a keel-edge pinhole collimator.

For a given SPECT application the desired or achievable FOV determines the pinhole magnification required. The magnification and intrinsic spatial resolution of the detector, in turn, determine the achievable system spatial resolution. The pinhole aperture size can be designed to provide the desired spatial resolution for a known pinhole magnification and detector configuration. The total system resolution $R_t$ for a pinhole system and detector with intrinsic spatial resolution $R_i$ is given by

$$R_t = \sqrt{R_{coll}^2 + \left(\frac{R_i}{M}\right)^2} \tag{4.6}$$

It can be shown that the most efficient (but not necessarily optimal) trade-off between resolution and sensitivity is obtained when the two terms in Eq. (4.6) are approximately equal, i.e.

$$R_{coll} = d_{\text{eff}}\left(1 + \frac{1}{M}\right) = \frac{R_i}{M} \tag{4.7}$$

Therefore, an efficient trade-off between sensitivity and resolution is achieved when the pinhole aperture size is

$$d_{\text{eff}} = \frac{R_i}{M+1} \tag{4.8}$$

Note, for pixelated sensors the pixels are square and the response is discrete. Then, $d_{eff}$ can be chosen to be somewhat larger than that specified by Eq. (4.8). Equation (4.8) also tells us that for a given intrinsic detector resolution $R_i$, when magnification $M$ is increased the aperture size needs to be decreased accordingly to achieve the most efficient trade-off between resolution and sensitivity. Theoretically one can continue increasing magnification to improve resolution, however magnification cannot be increased without limit. The first limit comes from the size of the object to be imaged, which constrains the pinhole to AOR distance, and the configuration of the SPECT system, which constrains the focal length of the pinhole. The second limit is the size of the FOV. If $b$ is too small (pinhole too close to the object), truncation of projections may occur. Thus, there is a limit to the extent to which adjustment of a single pinhole parameter can achieve the desired trade-off between resolution and sensitivity.

### 3.6.3 Multi-Pinhole Collimation

In many cases, the constraints on magnification mean that the projection of the object occupies a small proportion of the available detector area and the remaining detector area is wasted. To make more efficient use of the detector and, in turn,

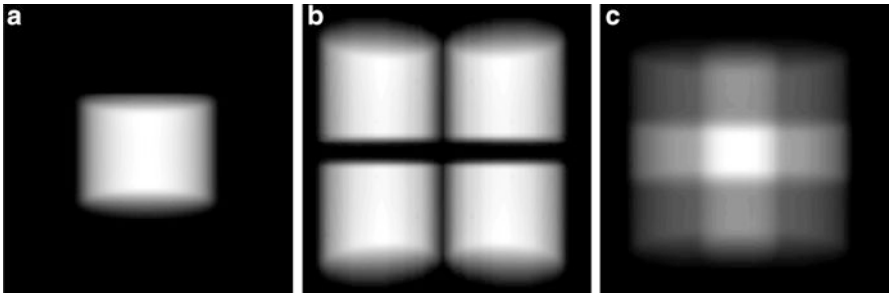


**Fig. 4.6** Projections of a simulated cylinder through (**a**) one pinhole, (**b**) four pinholes without multiplexing and (**c**) four pinholes with multiplexing

increase sensitivity, one can employ multiple pinholes to project additional projections of the object onto the available detector area. Multiple pinhole collimators can be designed such that they produce overlapping or non-overlapping projections of the object on the detector (Fig. 4.6). When the projections overlap, the acquired data are said to be multiplexed, which means that detector elements in the overlap region record data from more than one channel (i.e. more than one ray path). Thus, the data in the overlap region are ambiguous.

At first, such ambiguity may be thought to be problematic with regard to producing an accurate artefact-free reconstruction of the object. However, provided the projection data acquired from all angles are consistent with each other, the object can be faithfully reconstructed from multiplexed data (Fig. 4.7), although iterative algorithms typically take longer to converge compared with non-multiplexed data. The key question is whether the additional sensitivity in the overlap region outweighs the increased noise due to slower convergence. We shall return to this question after considering the effects of multiplexing and inconsistent projections and how to avoid them.

In Fig. 4.7a, the condition of an inconsistent projection is shown. The part labelled "inconsistently projected volume" in the object is projected to the detector through pinhole 2 (PH2) but not through pinhole 1 (PH1). As a result, the part of the multiplexed region indicated by the dashed line is formed by inconsistent projections. When reconstruction is performed, back projection errors arise from the missing projection of the "inconsistently projected volume" through pinhole 1, i.e. the back projection through PH1 would evaluate the inconsistently projected volume as zero, while the back projection through PH2 would not. This inconsistency makes it difficult or impossible for the iterative algorithm to match the multiplexed part correctly during forward projection. As a result, the reconstructed image may contain artefacts, or the iterative algorithm may never converge.

Thus, if a multi-pinhole collimator allows multiplexing, it should be designed in such a way that the imaging volume is projected consistently through all pinholes. To address the problem of an inconsistently projected volume, one can employ

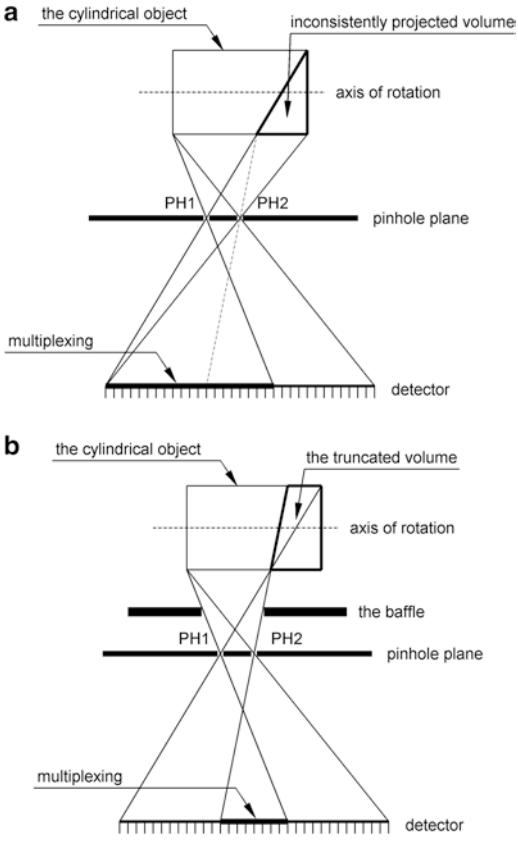


**Fig. 4.7** Effects of multiplexing and inconsistent projections in multi-pinhole collimation. Multiplexing arises when parts of the object project through different pinholes into the same area of the detector. (**a**) Inconsistency arises when different parts of the object are partially projected through each of the pinholes. (**b**) These effects can be mitigated by including appropriate shielding (i.e. a baffle) to minimise overlap and inconsistency

focused pinholes or insert a gamma ray absorbing baffle in front of the pinhole plate as shown in Fig. 4.7b. By blocking some of the projections from PH2, inconsistent projections are effectively removed from the multiplexed region, and at the same time multiplexing is reduced [45].

There have been detailed theoretical and numerical simulation studies to investigate the image quality trade-offs associated with multiplexed and non-multiplexed designs [46, 47], but the value of multiplexing remains an open question. However, one clear advantage that multiple pinhole collimation (with or without overlapping) has over single pinhole designs is that it improves sampling in the axial direction. According to Tuy's condition [15], when single pinhole collimation is used projection data in the off-axis slices (the top and bottom parts of the coronal image) are incompletely sampled. Only the central region is properly sampled. This problem is largely overcome by positioning multiple pinholes such that they increase sampling along the axial direction.

### 3.6.4 Slit–Slat Collimation

Slit–slat collimation is a combination of pinhole (slit) and fan-beam (slat) designs. It may be suitable for SPECT imaging of medium sized animals where the optimal sensitivity and FOV lie between converging multi-channel and pinhole collimation for a specified spatial resolution. A narrow slit is positioned close to the object aligned with the AOR. The image of the object is magnified through the slit, as in pinhole geometry. Between the slit and detector are positioned a series of thin slats aligned perpendicular to the AOR. The slats behave like the septa of a multi-channel collimator, providing complete sampling in the axial direction. This addresses the limited off-axis sampling of circular orbit single pinhole SPECT where there is insufficient data to avoid reconstruction artefacts. The slit provides magnification and improved spatial resolution in the transaxial direction and high sensitivity for objects close to the slit, like a pinhole collimator. The axial resolution is less than that of an equivalent pinhole design because of the distance between the object and the slats [48].

Zeng [41] proposed a modified slit–slat design for small animal SPECT imaging, referred to as 'skew-slit' collimation. A vertical slit is aligned with the AOR and positioned close to the object, providing magnification in the transaxial direction. Between the vertical slit and collimator are positioned a number of horizontal slits. These provide no magnification in the axial direction, as the distance of the vertical slits from the object and the collimator are identical. The distance between the horizontal slits maximises the detector area but reduces overlapping of the projection data. Initial simulation and phantom results demonstrate an improvement in reconstructed transaxial spatial resolution over the multi-pinhole design [41].

## 4 SPECT Image Reconstruction

Tomographic data are reconstructed from a series of 2D projections into a 3D volume, allowing visualisation of the radiopharmaceutical distribution without interference from over- and underlying activity. There are two broad categories of tomographic reconstruction methods for emission tomography, analytic and iterative [49]. The main analytic method is filtered backprojection (FBP) [50, 51], which is a discrete implementation of a mathematical solution that is exact for noiseless and continuous functions [52]. However, real SPECT data is neither noiseless nor continuous. Thus analytical methods, although computationally efficient, are limited in their ability to deal with noisy data, finite discrete linear sampling and photon attenuation [53, 54]. Iterative methods, such as maximum likelihood expectation maximization (ML-EM) [55, 56] require greater computation than analytic methods but they use an appropriate statistical model to describe the data. They also allow for more realistic modelling of physical effects such as scatter, attenuation and detector properties, resulting in a potentially more accurate representation of the radiopharmaceutical distribution within the subject. Iterative methods have become routinely used in both PET and SPECT due to rapid improvements in computational power and the advantages they confer.

The FBP method of tomographic reconstruction is commonly used with parallel ray geometry such as that encountered with parallel hole collimation in SPECT. It can also be adapted for converging ray geometries such as fan beam and cone beam X-ray CT. However, in small animal SPECT using single and multiple pinhole geometries, iterative algorithms based on EM and its variants are much more commonly used.

The ML-EM method starts with an initial estimate of the object to be reconstructed, usually a uniform cylinder. The estimate of the object is forward projected to create a series of estimated projection data. The forward projection may include modelling of scatter, attenuation, collimator and detector response, and the ML-EM method explicitly models Poisson noise. The estimated and measured projection data are compared (cost function), and the difference is expressed as a ratio (projection space error) which is backprojected (image space error) and multiplied by the previous volume estimate (update step). The process is then repeated iteratively until the projection space error reduces to an acceptably small value or the reconstructed volume reaches an acceptable solution [49, 54]. The ML-EM algorithm is guaranteed to converge to a maximum likelihood solution but since the projection data are noisy, that may mean fitting primarily to the noise if the algorithm is allowed to continue for too many iterations. Thus, it is common to either terminate the algorithm early in the iterative process or, preferably, to post smooth the reconstruction after it has substantially converged [57].

Ordered subsets expectation maximisation (OS-EM) is a modification of ML-EM which speeds up the reconstruction process [58]. SPECT projections are organised into groups of symmetric projections which represent subsets of the total number of projections, e.g. 64 projections can be divided into 2, 4, 8, 16 or 32 subsets. Subsets of 1 and 64 can also be used, but these are equivalent to ML-EM and multiplicative algebraic reconstruction technique (MART) [59] respectively. Forward projection, back projection and update steps are performed using all projections within a given subset. The process is repeated in a sequence that maximises the spread of subsets around the object (referred to as subset balance), until all subsets have been forward and back projected. This is referred to as one full iteration of OS-EM, which consists of several updates (equivalent to the number of subsets) to the volume estimate. It has been demonstrated that one iteration of OS-EM is almost exactly equivalent to $N$ iterations of ML-EM where $N$ is the number of subsets, hence it accelerates the reconstruction by a factor of approximately $N$ [58]. OS-EM combines the benefits of ML-EM with greatly improved processing speed, making it an important algorithm for SPECT reconstruction [49, 58].

## 5 State-of-the-Art Pre-clinical SPECT Systems

At the time of writing there are six small animal SPECT systems available commercially. These systems encompass a wide variety of detector and collimator designs, covering most of the technologies discussed in this chapter. Most are also

**Table 4.2** Commercial small animal SPECT systems and the technologies they employ

| System | Detector | Photodetector | Collimation |
|---|---|---|---|
| X-SPECT | CZT | N/a | Single or multiple pinhole |
| EXplore speCZT | CZT | N/a | Multi-slit or multi-pinhole |
| NanoSPECT | Monolithic NaI(Tl) | PMT | Multi-pinhole with multiplexing |
| U-SPECT-II [5] | Monolithic NaI(Tl) | PMT | Multiple focussed pinholes |
| Inveon SPECT | Pixelated NaI(Tl) | PS-PMT | Single and multi-pinhole |
| YAP-(S)PET | Pixelated YAP:Ce | PS-PMT | Parallel hole |

available as dual modality SPECT/CT systems and, in the case of the YAP-(S)PET system, as a dual purpose SPECT–PET scanner. The commercial systems and the technologies they employ are listed in Table 4.2. The performance specifications are not included as these are dependent on several variable parameters, including the pinhole aperture diameter (most systems offer several choices for different applications) and radius of rotation. Nor have the companies marketing these systems been included, mainly because such information is subject to change and likely to become out of date quickly. However, all these systems are capable of achieving sub-millimetre spatial resolution with a FOV suitable for mice and/or rats and most have sufficient temporal sampling and sensitivity for performing kinetic studies. All systems offer both analytical and iterative 3D OS-EM reconstruction as a minimum, with at least some form of system modeling such as spatially variant point source response modeling.

## 6 Summary and Future Perspectives

Small animal SPECT systems have come a long way since the first converted clinical systems were used to image laboratory animals using pinhole collimation in the early 1990s [23, 25, 36]. After two decades of continuous development, dedicated small animal SPECT systems are routinely being used in research laboratories and the pharmaceutical industry to image a wide range of animal models with an equally wide range of labelled compounds at sub-millimetre spatial resolution.

It is interesting to note that most of the commercially available systems still use the same basic form of collimation used in the early prototypes, i.e. pinhole collimation, and some still use large area monolithic NaI(Tl) detectors with conventional photomultiplier tubes. Nevertheless, several of the novel technologies discussed in this chapter have found their way into commercial systems, including pixelated scintillators, semiconductor detectors, position sensitive photodetectors and multi-pinhole collimation and reconstruction.

It is difficult to predict what future technologies might be around the corner, but it is possible to make some general observations. First, despite the impact of novel multi-pinhole designs and associated image reconstruction developments, the main challenge for small animal SPECT remains increasing the sensitivity of these

systems. This is an important goal for two reasons: (1) the radiation dose to experimental animals is relatively high and needs to be reduced to enable longitudinal studies to be performed on the same animal; (2) for the full potential of small animal SPECT to be realised, higher sensitivity is needed to ensure accurate quantification of tracer kinetics and associated physiological parameters.

The second observation is that it continues to be the case that experimental small animal imaging systems are an ideal platform for testing new technologies. Many of the technologies discussed in this chapter, including pixelated detectors and position sensitive photodetectors, were incorporated into early prototype small animal imaging systems, both SPECT and PET. It is also worth noting that some new technologies like CZT are better suited to the relatively low gamma ray energies of single photon emitters than PET. CZT is also more likely to be used in small animal systems than clinical systems in the near future because growing large uniform detectors with this semiconductor material remains a significant manufacturing challenge.

Finally, multimodality imaging has made a major impact on both the pre-clinical and clinical realms [60]. SPECT/CT is widely available and is almost essential for optimal interpretation and quantification of the radiopharmaceutical distribution. Several laboratories are also developing combined SPECT and optical imaging systems. The current major challenge is to develop stable, reliable SPECT/MRI systems that combine the advantages of both modalities without compromising the performance of either. With the recent developments in solid state radiation detectors, photodetectors and low noise multi-channel amplifiers, such systems are not far away.

## References

1. Hevesy G, Chiewitz O (1935) Radioactive indicators in the study of phosphorous metabolism in rats. Nature 136:754–755.
2. Jansen FP, Vanderheyden J-L (2007) The future of SPECT in a time of PET. Nucl Med Biol 34:733–735.
3. Acton PD, Choi SR, Plossl K, Kung HF (2002) Quantification of dopamine transporters in the mouse brain using ultra-high resolution single-photon emission tomography. Eur J Nucl Med Mol Imaging 29:691–8.
4. Pissarek MB, Oros-Peusquens AM, Schramm NU (2008) Challenge by the murine brain: multi-pinhole SPECT of $^{123}$I-labelled pharmaceuticals. J Neurosci Meth 168:282–92.
5. van der Have F, Vastenhouw B, Ramakers RM, Branderhorst W, Krah JO, Ji C, et al. (2009) U-SPECT-II: An Ultra-High-Resolution Device for Molecular Small-Animal Imaging. J Nucl Med 50:599–605.
6. Zhou R, Thomas DH, Qiao H, Bal HS, Choi SR, Alavi A, et al. (2005) In vivo detection of stem cells grafted in infarcted rat myocardium. J Nucl Med 46:816–22.
7. Beekman FJ, van der Have F (2007) The pinhole: gateway to ultra-high-resolution three-dimensional radionuclide imaging. Eur J Nucl Med Molec Imaging 34:151–161.
8. Acton PD, Kung HF (2003) Small animal imaging with high resolution single photon emission tomography. Nucl Med Biol 30:889–95.
9. Loudos GK (2007) Advances in small animal imaging systems. AIP Conference Proceedings 958:127–30.

10. Funk T, Sun M, Hasegawa BH (2004) Radiation dose estimate in small animal SPECT and PET. Med Phys 31:2680–6.
11. Beekman FJ, van der Have F, Vastenhouw B, van der Linden AJA, van Rijk PP, Burbach JPH, et al. (2005) U-SPECT-I: A Novel System for Submillimeter-Resolution Tomography with Radiolabeled Molecules in Mice. J Nucl Med 46:1194–1200.
12. Hwang AB, Taylor CC, VanBrocklin HF, Dae MW, Hasegawa BH (2006) Attenuation correction of small animal SPECT images acquired with<sup>125</sup>I-iodorotenone. IEEE Trans Nucl Sci 53:1213–20.
13. Li J, Jaszczak RJ, Coleman RE (1995) Quantitative small field-of-view pinhole SPECT imaging: initial evaluation. 1994 Nuclear Science Symposium and Medical Imaging Conference, NSS/MIC. Norfolk, VA, 30 Oct.-5 Nov., pp.
14. Acton PD, Kushner SA, Kung MP, Mozley PD, Plossl K, Kung HF (1999) Simplified reference region model for the kinetic analysis of [99mTc]TRODAT-1 binding to dopamine transporters in nonhuman primates using single-photon emission tomography. Eur J Nucl Med 26: 518–26.
15. Tuy HK (1983) An Inversion-Formula for Cone-Beam Reconstruction. Siam J Appl Math 43:546–552.
16. Metzler SD, Bowsher JE, Jaszczak RJ (2003) Geometrical similarities of the Orlov and Tuy sampling criteria and a numerical algorithm for assessing sampling completeness. IEEE Trans Nucl Sci 50:1550–5.
17. Acton PD, Hou C, Kung MP, Plossl K, Keeney CL, Kung HF (2002) Occupancy of dopamine D2 receptors in the mouse brain measured using ultra-high-resolution single-photon emission tomography and [123]IBF. Eur J Nucl Med Molec Imaging 29:1507–15.
18. Habraken JBA, de Bruin K, Shehata M, Booij J, Bennink R, van Eck Smit BLF, et al. (2001) Evaluation of High-Resolution Pinhole SPECT Using a Small Rotating Animal. J Nucl Med 42:1863–1869.
19. Goertzen AL, Jones DW, Seidel J, King Li AKL, Green MVAGMV (2005) First results from the high-resolution mouseSPECT annular scintillation camera. IEEE Trans Med Imaging 24:863–867.
20. Shannon CE (1949) Communication in the presence of noise. Proc IRE 37:10–21.
21. Rosenthal MS, Cullom J, Hawkins W, Moore SC, Tsui BMW, Yester M (1995) Quantitative SPECT Imaging: A Review and Recommendations by the Focus Committee of the Society of Nuclear Medicine Computer and Instrumentation Council. J Nucl Med 36:1489–1513.
22. Hutton B (1996) Angular Sampling Necessary for Clinical SPECT. J Nucl Med 37:1915–1916.
23. Jaszczak RJ, Li J, Wang H, Zalutsky MR, Coleman RE (1994) Pinhole collimation for ultra-high-resolution, small-field-of-view SPECT. Phys Med Biol 39:425–437.
24. Anger HO (1958) Scintillation Camera. Rev Sci Instrum 29:27–33.
25. Weber DA, Ivanovic M, Franceschi D, Strand SE, Erlandsson K, Franceschi M, et al. (1994) Pinhole SPECT: An approach to in vivo high resolution SPECT imaging in small laboratory animals. J Nucl Med 35:342–348.
26. Barrett HH, Hunter WCJ (2005) Detectors for small-animal SPECT I. Overview of Technologies. In: Kupinski MA, Barrett HH, eds. *Small animal SPECT imaging*. New York: Springer, pp.
27. Schramm N, Wirrwar A, Sonnenberg F, Halling H (2000) Compact high resolution detector for small animal SPECT. IEEE Trans Nucl Sci 47:1163–1167.
28. Meikle SR, Kench P, Weisenberger AG, Wojcik R, Smith MF, Majewski S, et al. (2002) A prototype coded aperture detector for small animal SPECT. IEEE Trans Nucl Sci 49:2167–71.
29. Wirrwar A, Schramm N, Halling H, Muller-Gartner HW (2000) The optimal crystal geometry for small-field-of-view gamma cameras: arrays or disks? Nuclear Science Symposium Conference Record, 2000 IEEE, vol. 3, pp. 21/91-21/93 vol.3.
30. Wirrwar A, Schramm N, Vosberg H, Muller-Gartner HW (1999) Influence of crystal geometry and wall reflectivity on scintillation photon yield and energy resolution. Nuclear Science Symposium, 1999. Conference Record. 1999 IEEE, vol. 3, pp. 1443–1445 vol.3.

31. MacDonald LR, Patt BE, Iwanczyk JS, Tsui BMW, Wang Y, Frey EC, et al. (2001) Pinhole SPECT of mice using the LumaGEM gamma camera. IEEE Trans Nucl Sci 48:830–836.
32. Stevenson G (2005) The animal in animal imaging. In: Kupinski MA, Barrett HH, eds. *Small Animal SPECT Imaging*. New York: Springer, pp 87–100.
33. Meikle SR, Kench P, Wojcik R, Smith MF, Weisenberger AG, Majewski S, et al. (2003) Performance evaluation of a multipinhole small animal SPECT system Nuclear Science Symposium Conference Record, IEEE. Volume 3, 19–25 Oct. 2003 Page(s):1988–1992, 19–25 Oct., vol. 3, pp. 1988–1992.
34. Zimmerman RE, Moore SC, Mahmood A (2004) Performance of a triple-detector, multiple-pinhole SPECT system with iodine and indium isotopes. Nuclear Science Symposium Conference Record, 2004 IEEE, vol. 4, pp. 2427–2429.
35. Forrer F, Valkema R, Bernard B, Schramm N, Hoppin J, Rolleman E, et al. (2006) In vivo radionuclide uptake quantification using a multi-pinhole SPECT system to predict renal function in small animals. Eur J Nucl Med Molec Imaging 33:1214–1217.
36. Ishizu K, Mukai T, Yonekura Y, Pagani M, Fujita T, Magata Y, et al. (1995) Ultra-high resolution SPECT system using four pinhole collimators for small animal studies.[see comment]. J Nucl Med 36:2282–7.
37. Metzler SD, Jaszczak RJ, Patil NH, Vemulapalli S, Akabani G, Chin BB (2005) Molecular imaging of small animals with a triple-head SPECT system using pinhole collimation. IEEE Trans Med Imaging 24:853–862.
38. Furenlid LR, Wilson DW, Yi-chun C, Hyunki K, Pietraski PJ, Crawford MJ, et al. (2004) FastSPECT II: a second-generation high-resolution dynamic SPECT imager. IEEE Trans Nucl Sci 51:631–5.
39. Izaguirre EW, Mingshan S, Vandehei T, Despres P, Yong H, Funk T, et al. (2006) Evaluation of a Large Pixellated Cadmium Zinc Telluride Detector for Small Animal Radionuclide Imaging. Nuclear Science Symposium Conference Record, 2006. IEEE 6:3817–3820.
40. Seo HK, Choi Y, Kim JH, Im KC, Woo SK, Choe YS, et al. (2000) Performance evaluation of the plate and array types of NaI(Tl), CsI(Tl) and CsI(Na) for small gamma camera using PSPMT. Nuclear Science Symposium Conference Record, 2000 IEEE, vol. 3, pp. 21/94-21/97 vol.3.
41. Zeng GL (2008) A skew-slit collimator for small-animal SPECT. J Nucl Med Technol 36:207–12.
42. Tenney CR (2000) Gold pinhole collimators for ultra-high resolution Tc-99m small volume SPECT. IEEE Nuclear Science Symposium., Piscataway, NJ, USA., vol. 3, pp. 22/44-6.
43. Tenney CR, Tornai MP, Smith MF, Turkington TG, Jaszczak RJ (2001) Uranium pinhole collimators for 511-keV photon SPECT imaging of small volumes. IEEE Trans Nucl Sci 48:1483–9.
44. Tenney CR (2004) Pinhole edge penetration and scatter in small-animal energy-integrating pinhole emission computed tomography. 2003 IEEE Nuclear Science Symposium. Conference Record. Portland, OR, 19–25 Oct., pp.
45. Kench PL, Lin J, Gregoire MC, Meikle SR (2011) An investigation of inconsistent projections and artefacts in multi-pinhole SPECT with axially aligned pinholes. Phys Med Biol 56:7487–7503.
46. Rentmeester MCM, Have Fvd, Beekman FJ (2007) Optimizing multi-pinhole SPECT geometries using an analytical model. Phys Med Biol 52:2567–2581.
47. Vunckx K, Bequé D, Defrise M, Nuyts J (2008) Single and multipinhole collimator design evaluation method for small animal SPECT. IEEE Trans Med Imaging 27:36–46.
48. Metzler SD, Accorsi R, Novak JR, Ayan AS, Jaszczak RJ (2006) On-Axis Sensitivity and Resolution of a Slit-Slat Collimator. J Nucl Med 47:1884–1890.
49. Wernick MN, Aarsvold JN (2004) *Emission Tomography. The Fundamentals of PET and SPECT*. San Diego: Elsevier Academic Press.
50. Bracewell RN (1956) Strip integration in radio astronomy. Aust J Phys 9:198–217.
51. Ramachandran GN, Lakshminarayanan AV (1971) Three-dimensional reconstruction from radiographs and electron micrographs: Application of convolutions instead of Fourier transforms. Proc Nat Acad Sci 68:2236–2240.

52. Radon J (1917) Über die Bestimmung von Funktionen durch ihre Integralwerte längs gewisser Mannigfaltigkeiten. Berichte Sächsische Akademie der Wissenschaften, Leipzig. Mathematisch - Physikalische Klasse 69:262–277.
53. Madsen MT (2007) Recent advances in SPECT imaging. J Nucl Med 48:661–673.
54. Cherry SR, Sorenson JA, Phelps ME (2003) *Physics in Nuclear Medicine*, 3 ed. Philadelphia: Saunders.
55. Shepp LA, Vardi Y (1982) Maximum likelihood reconstruction for emission tomography. IEEE Trans Med Imaging MI-1:113–22.
56. Lange K, Carson R (1984) EM reconstruction algorithms for emission and transmission tomography. J Comput Assist Tomogr 8:306–16.
57. Nuyts J, Fessler JA (2003) A penalized-likelihood image reconstruction method for emission tomography, compared to postsmoothed maximum-likelihood with matched spatial resolution. IEEE Trans Med Imaging 22:1042–1052.
58. Hudson HM, Larkin RS (1994) Accelerated image reconstruction using ordered subsets of projection data. IEEE Trans Med Imaging 13:601–609.
59. Gordon R, Bender R, Herman GT (1970) Algebraic reconstruction techniques (ART) for three-dimensional electron microscopy and x-ray photography. J Theoret Biol 29:471–481.
60. Townsend DW, Cherry SR (2001) Combining anatomy and function: the path to true image fusion. Eur Radiol 11:1968–1974.